

## Direct observation of domain wall evolution at a bifurcation in magnetic network structures

Chandrasekhar Murapaka<sup>1</sup>, Pankaj Sethi<sup>1</sup>, Sarjoosing Goolaup<sup>1</sup>, Ramu Maddu<sup>1</sup>, Yunjie Chen<sup>2</sup>, Siang Huei Leong<sup>2</sup>, and Wen Siang Lew<sup>1\*</sup>

<sup>1</sup>School of Physical and Mathematical Sciences, Nanyang Technological University, 21 Nanyang Link, Singapore 637371

<sup>2</sup>Data Storage Institute, (A\*STAR) Agency for Science, Technology and Research, DSI Building, 5 Engineering Drive 1, Singapore 117608

E-mail: wensiang@ntu.edu.sg

Received August 20, 2014; accepted September 25, 2014; published online October 16, 2014

We report on the magnetization dynamics at a bifurcation in a dual-branch magnetic network structure. When a transverse domain wall (DW) propagates through the network, interaction with an edge defect at the bifurcation leads to the transformation of the DW from transverse to vortex. The topological charge is conserved as the DW moves through the bifurcation, and this charge conservation is intrinsically linked to a  $-1/2$  topological defect in the system. Magnetic force microscopy (MFM) imaging enables the direct observation of defect displacement during DW transformation, which induces a selective switching in the branch of the network structure. © 2014 The Japan Society of Applied Physics

The controlled motion of domain walls (DWs) in magnetic nanowires has opened up new avenues towards solid-state nonvolatile magnetic memory<sup>1)</sup> and logic devices.<sup>2)</sup> Recent proposals of DW logic devices have considered the motion of the DWs to carry out logic operations on patterned nanowire networks.<sup>2)</sup> Nanowire networks have also been shown to be an ideal candidate for analogous spin-ice systems.<sup>3–5)</sup> The magnetic properties of ferromagnetic networks can be described in terms of the uniform magnetization of each wire and the interaction at the vertices. The magnetization reversal in these structures is via the emission of a DW from a vertex. The dynamics of the DW in the network strongly correlates with the charge at the vertex in the network.<sup>6)</sup> The DW may either annihilate or a new DW may subsequently be emitted depending on the vertex charge. In addition to the magnetic charge, the DW can also be represented as the composite of topological edge defects.<sup>7)</sup> For instance, a vortex wall is a combination of two  $-1/2$  edge defects (vertices) and one  $+1$  bulk defect (core). A transverse DW is a composite of two half-integer edge defects with their positions dependent on the chirality of the DW. Recently, Pushp et al. have shown that the trajectory of a vortex DW in an interconnected network structure is highly dependent on the chirality of the DW.<sup>8)</sup> The interaction of the vortex and a Y-shaped junction is governed by topological charge conservation. The vortex DW conserves its chirality and structure as it moves through the network. In the case of the transverse DW, it was shown that the motion of a DW in a network follows a nonrandom path distribution.<sup>9)</sup> This was attributed to the chirality of the DW. The DW interaction at the vertex leads to the formation of a “C”-like state, followed by the subsequent motion in the network.

In this study, we elucidate the magnetization dynamics at a bifurcation in a dual-branch or Y-shaped network structure. Magnetic force microscopy (MFM) imaging reveals that the motion of the transverse domain wall (TDW) through the network structure can lead to a chirality-dependent selective switching in the branch. Micromagnetic simulations show that the injected TDW undergoes complex transformations and, in the process, reallocates the edge defects at the bifurcation.

The magnetization reversal process of the network structure was first investigated using OOMMF micromagnetic simulations.<sup>10)</sup> The widths of the nanowire conduits before and after the bifurcation are chosen to be 100 nm to ensure that TDWs are the only stable configurations. Each branch

deviates at an angle  $\phi = 70^\circ$  from the nanowire long axis ( $x$ -axis). The following material parameters of Permalloy  $\text{Ni}_{80}\text{Fe}_{20}$  were considered for the given structure: the exchange constant  $A = 1.3 \times 10^{-11}$  J/m, saturation magnetization  $M_s = 860 \times 10^3$  A/m, and anisotropy constant  $K = 0$  J/m<sup>3</sup>. The Gilbert damping coefficient  $\alpha$  was set as 0.01. The unit cell size was chosen to be  $5 \times 5 \times 5$  nm<sup>3</sup> in the  $x$ -,  $y$ -, and  $z$ -axes.

Figure 1(a) depicts the schematic of the magnetization configuration of the network structure as a tail-to-tail DW with an “up” chirality (TT-U) that propagates along the nanowire conduit. A magnetic field is applied to move the DW through the network structure and selectively switch the magnetization of the lower branch, as shown in Fig. 1(b). To understand the DW selective movement along the lower branch structure, we have extracted the spin state evolution of the DW at the bifurcation. The corresponding spin states, as obtained by micromagnetic simulation, are shown in Fig. 1(c-i–iii). The DW motion from the bifurcation to the lower branch is completed via a complex DW transformation. The magnetization switching is governed by the conservation of the topological edge defects. Schematic representations of the elementary defects with  $+1/2$  and  $-1/2$  winding numbers are shown in Fig. 1. A defect with all spins diverging is assigned a  $+1/2$  winding number, whereas a defect with two spins diverging and one spin converging is assigned with a  $-1/2$  winding number.<sup>7)</sup> A TT-U has a  $-1/2$  winding number at the top edge and a  $+1/2$  winding number at the bottom edge of the DW, as seen in Fig. 1(c-i). At the bifurcation, a vertex, which is characterized by a  $-1/2$  winding number, is observed. When the DW reaches the bifurcation, it is pinned before interacting with the vertex state. A TDW with an up chirality has a clockwise spin orientation.<sup>11)</sup> When the DW reaches the bifurcation, the spins adopt a clockwise orientation, which in turn pushes the vertex core towards the upper branch. The DW has a higher energy at the  $+1/2$  edge defect than at the  $-1/2$  edge defect owing to the transverse variation in DW width.<sup>7,12,13)</sup> With the increase in magnetic field strength, the bottom part of the DW depins and collides with the vertex at the bifurcation. The collision between the transverse DW and the edge defect at the vertex leads to the formation of a vortex DW with a clockwise orientation. The conservation of topological charge dictates that the total winding number of edge defects should be conserved during DW interaction or transformation.<sup>8)</sup> The vortex DW is characterized by a  $+1$  bulk defect at the core

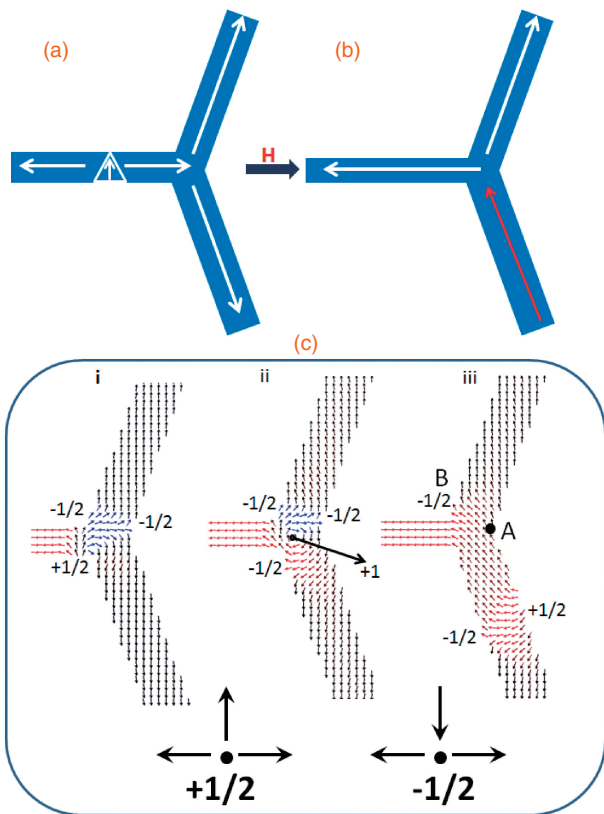


**Fig. 1.** Schematics of the magnetization orientations in the network structure when a tail-to-tail transverse DW with an up chirality (TT-U) is injected: (a) before and (b) after the TT-U propagates through the bifurcation. (c-i-iii) Images of the simulated magnetization configurations during the reversal process, which are labeled with the corresponding winding numbers of edge defects. Point A indicates the position of the vortex at the bifurcation where the annihilation of the vortex core occurs. Point B represents the final position of the edge defect  $n = -1/2$  at the bifurcation. Shown below are the schematic representations of elementary edge defects with  $+1/2$  and  $-1/2$  winding numbers.

and two  $-1/2$  defects at the edges. In this system, the transformation of the  $+1/2$  defect from the TT-U to a  $+1$  defect leads to the formation of the vortex configuration. To conserve the total winding number of the system, a  $-1/2$  defect is nucleated along the same edge of the transformed  $+1/2$  defect, as shown in Fig. 1(c-ii). A further increase in magnetic field strength causes the core of the vortex DW to move towards point A, where the core eventually annihilates. To maintain the total topological charge at the bifurcation, the annihilation of the vortex core ( $+1$  defect) leaves behind a  $-1/2$  edge defect from the TT-U at the bifurcation and a new TDW is nucleated within the lower branch, as shown in Fig. 1(c-iii). The motion of the TDW through the lower branch switches the magnetization. The DW motion through the network structure displaces the edge defect from positions A to B. This shows that the total topological winding number is always  $-1/2$  before and after the DW motion through the dual-branch structure.

To investigate the effect of DW chirality on the reversal process, a tail-to-tail DW with a “down” chirality (TT-D) is relaxed in the nanowire, as shown in Fig. 2(a). The magnetization switching of the TT-D follows the same process as the TT-U. However, when the DW is driven through the Y-shaped structure, the TT-D selectively travels through the upper branch and switches its magnetization, as shown

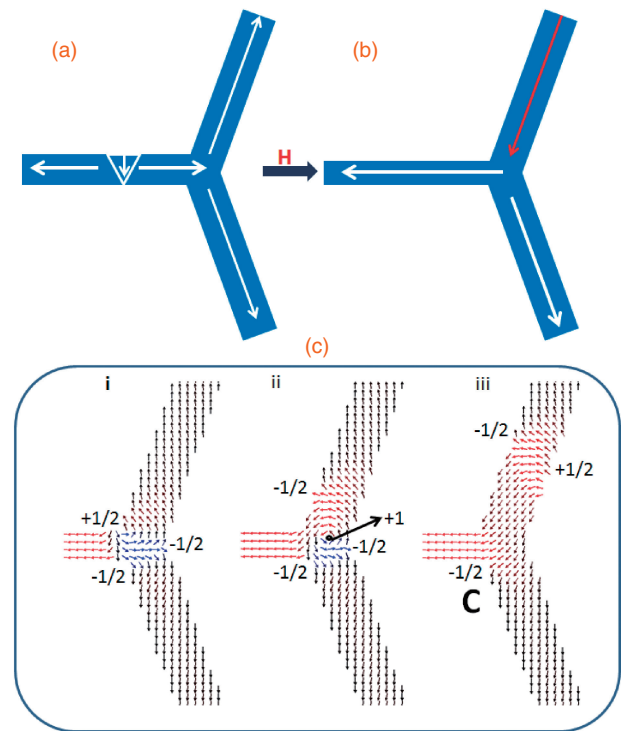


**Fig. 2.** Schematics of the magnetization orientations in the network structure when a tail-to-tail transverse DW with a down chirality (TT-D) is injected: (a) before and (b) after the TT-D propagates through the bifurcation. (c-i-iii) Images of the simulated magnetization configurations during the reversal process with winding numbers of the edge defects identified. Point “C” represents the final position of the edge defect  $n = -1/2$  at the bifurcation.

in Fig. 2(b). A TT-D is composed of a  $+1/2$  defect at the top edge and a  $-1/2$  defect at the bottom edge, as shown in Fig. 2(c-i). A similar TDW pinning at the bifurcation occurs when a magnetic field is applied. The spins in the TT-D always rotate in anticlockwise orientation.<sup>11)</sup> The spin relaxation at the bifurcation causes the edge defect at the vertex to be displaced towards the lower branch. The TDW depinning leads to the formation of an anticlockwise vortex DW. The DW transforms from a transverse configuration to a vortex configuration via the annihilation of the  $+1/2$  defect and the generation of a  $-1/2$  defect in the upper branch, as shown in Fig. 2(c-ii). An increase in magnetic field strength leads to the annihilation of the vortex DW, leaving behind the  $-1/2$  defect at the vertex position C and the nucleated TDW in the upper branch, as shown in Fig. 2(c-iii). The motion of this TDW towards the end of the upper branch switches the magnetization. The switching process displaces the edge defect from positions A to C. Thus, the arrangement of edge defects in the TDWs affects the reversal process of the branch structure. The DW always moves towards the branch at which a  $+1/2$  defect (of the TDW) is facing. This implies that depending on the chirality of the injected DW, the magnetization in the branch structure can be selectively switched. Simulations with an oblique field reveal that the maximum field misalignment at which selective switching still occurs is  $\pm 10^\circ$  with respect to the longitudinal nanowire axis. Any further field misalignment results in both the branches switching their magnetization. The transverse component of the field leads to magnetization saturation along the opposite branch.

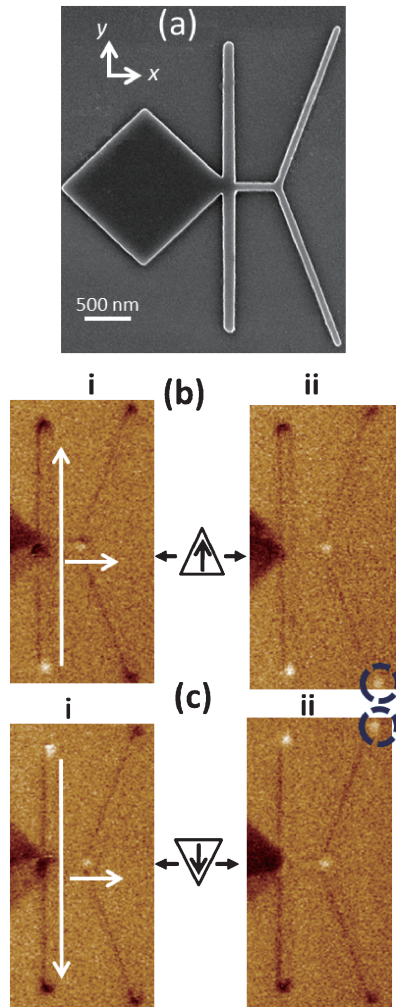


**Fig. 3.** (a) Scanning electron microscopy image of the fabricated network structure. (b-i) Magnetic force microscopy (MFM) image of the initial magnetization configuration of the structure when the chirality selector is saturated with a  $+y$  field and (b-ii) the final magnetization configuration after a TT-U is injected and driven towards the bifurcation. (c-i) MFM image of the initial magnetization configuration of the structure when the chirality selector is saturated with a  $-y$  field and (c-ii) the final magnetization configuration after a TT-D is injected and driven towards the bifurcation.

To substantiate the simulation results, we have experimentally investigated the DW dynamic behavior at a bifurcation in a Y-shaped magnetic network structure. Figure 3(a) shows a scanning electron microscopy image of the fabricated network structure. The structure is a thin film stack of Ta (5 nm)/Ni<sub>80</sub>Fe<sub>20</sub> (10 nm)/Ta (5 nm), deposited by DC magnetron sputtering at a base pressure of  $5 \times 10^{-8}$  Torr. The top and bottom Ta layers act as seed and capping layers for the NiFe film, respectively. The stack was patterned into the network structure using a combination of electron beam lithography and Ar-ion milling techniques. For DW injection and chirality selection mechanisms, a diamond-shaped NiFe nucleation pad with an area of  $2 \times 2 \mu\text{m}^2$ , together with a transverse nanowire, was attached to the left end of the nanowire. The transverse nanowire, which is  $4 \mu\text{m}$  long and  $100 \text{ nm}$  wide, acts as a chirality selector that is positioned between the nucleation pad and the nanowire. In the presence of a transverse nanowire, the DW has been shown to preserve its spin structure beyond the walker breakdown field. The DW fidelity length at an external field of  $50 \text{ Oe}$  has been

shown to be close to  $500 \text{ nm}$ .<sup>14)</sup> As such, the length of the longitudinal nanowire in our structure is chosen to be  $400 \text{ nm}$ . The chirality of the injected DW can be chosen on the basis of the initial magnetization of the transverse nanowire.<sup>13,14)</sup>

MFM imaging was carried out. First, the chirality selector is magnetized with a  $1 \text{ kOe}$  field along the  $y$ -direction meant to control the magnetization orientation of the selector. An injected DW can acquire an up or down chirality in the  $+y$ - or  $-y$ -direction depending on the magnetization orientation of the selector. Then, a  $1 \text{ kOe}$  field is applied along the  $+x$ -direction to magnetically saturate the network structure. To inject a TT DW into the nanowire conduit, a magnetic field is applied along the  $-x$ -direction. By increasing the field, the DW is nucleated in the pad, and the DW subsequently moves into the nanowire conduit after passing the chirality selector. The magnetization direction of the chirality selector remains unchanged during the field application along the  $x$ -direction because of the strong shape anisotropy along the  $y$ -direction.

As part of our experiments, multiple structures were fabricated and magnetic force microscopy imaging was carried out on all samples. A total of 20 scans were carried out for each sample. In all measurements, the initial configuration is as per the applied field. In 90% of our measurements, the final experimental results were the same as the simulation predictions. In the remaining cases, the upper and lower branches seemed to have switched and, very rarely, did the opposite branch switch. We presume that the switching of both branches is likely due to the field misalignment with respect to the sample. Our simulation results reveal that for a  $70^\circ$  branch, a misalignment of above  $\pm 10^\circ$  may result in the switching of both branches. In the other cases, we suspect that owing to the stochastic nature of the DW, a DW with an opposite chirality reaches the bifurcation.

Figure 3(b-i) shows the MFM image of the network structure when the selector and nanowire are saturated with the  $1 \text{ kOe}$  field along the  $+y$ - and  $+x$ -directions, respectively. The dark magnetic contrast shown at the top end point of the selector, as well as at each end point of the two output branches, indicates that the magnetizations are aligned along the  $+y$ - and  $+x$ -directions, respectively. When a  $50 \text{ Oe}$  field is applied along the  $-x$ -direction, a TT DW with an up chirality (TT-U) is injected from the pad to the nanowire conduit after passing through the selector. The DW propagates to the bifurcation of the network structure. However, such propagation stops at the bifurcation owing to pinning. When the field strength is increased to  $100 \text{ Oe}$ , the DW overcomes pinning and moves into one of the two branches. The MFM image in Fig. 3(b-ii) shows the eventual magnetic configuration. The MFM image shows that the magnetic contrast at the end point of the lower branch becomes bright, whereas that at the end point of the upper branch remains dark. This result implies that only the magnetization of the lower branch reverses the direction. Next, to verify the effect of the magnetization direction of the selector on branch switching, the selector-applied field was reversed to the  $-y$ -direction. The MFM image in Fig. 3(c-i) shows the initial magnetization configuration of the network structure after a similar  $+x$  saturation field application. The MFM image reveals that the top end point of the chirality selector shows a bright contrast, confirming the magnetization direction switch, while each end point of the two branches shows a dark contrast as before.

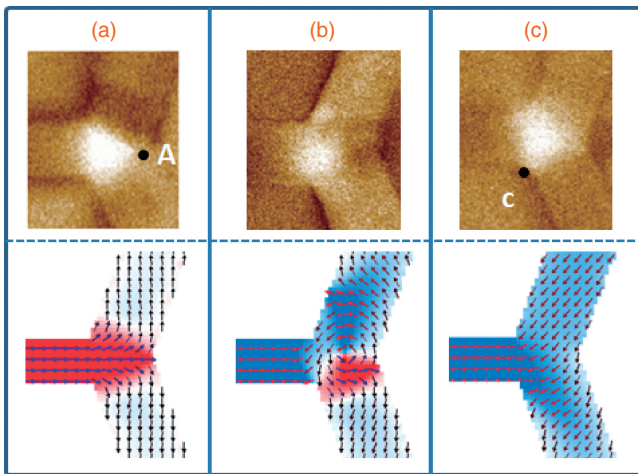


**Fig. 4.** (a) MFM image of the network structure at the bifurcation prior to the DW injection. (b) MFM image after the DW reaches the bifurcation and (c) MFM image of the bifurcation after the DW moves through the network structure. Below are the images of the simulated magnetization configurations.

Similarly, a DW injection field of 100 Oe was applied along the  $-x$ -direction to nucleate and drive the DW; in this case, a TT-DW was driven along the nanowire conduit before pinning at the bifurcation. The final magnetic configuration is shown in the MFM image in Fig. 3(c-ii). In contrast to the previous case, the magnetic contrast at the lower branch remains the same, whereas that of the upper branch changes from dark to bright, indicating a switch of the magnetization direction. This result clearly demonstrates that selective switching at either branch of the network structure can be obtained by controlling the chirality of the transverse DW. The MFM observation directly confirms the simulation results.

To observe the displacement of the edge defect at the bifurcation during the DW motion through the network, additional MFM scanning was carried out under a gradually increasing driving field with the injection of a TT-DW. The MFM image in Fig. 4(a) shows the magnetization configuration at the bifurcation prior to the DW injection. The triangular shape of the magnetization configuration clearly shows the vertex magnetization that separates the opposite magnetization directions of the two branches. The edge defect  $n = -1/2$  can be seen at point A. When the DW is injected and driven towards the bifurcation, the magnetization configuration becomes a vortex configuration, which can be seen as a circular magnetic contrast in the MFM image in Fig. 4(b). The magnetic contrast is relatively low, which can be attributed to the flux closure at the vortex.<sup>15</sup> The obtained MFM results support the explanation of the DW transformation, which is from a transverse configuration to a

vortex configuration, adhering to the principle of the conservation of topological charge. A further increase in magnetic field strength results in the DW selectively moving along one of the branches. As shown in Fig. 4(c), the edge defect is now at point C at the bifurcation. This is a direct evidence of the edge defect displacement and the conservation of topological charge at the bifurcation during the DW motion through the network structure.

In conclusion, the dynamic behavior of a transverse DW at a bifurcation in a magnetic network structure was investigated. The field-driven TDW motion in the network structure was found to be chirality-dependent. The magnetization switching at the bifurcation follows the conservation of the total edge defect winding number. The DW transforms from a transverse configuration to a vortex configuration at the bifurcation owing to the interaction with magnetization at the vertex. The annihilation of the vortex DW at a large field selectively nucleates a TDW in one of the two branches. The motion of the TDW through the network displaces the edge defect at the bifurcation. The chirality-dependent reversal process in the network structure assists in tracing the chirality of the injected TDW. Therefore, this structure can potentially be employed as a transverse DW chirality detector.

**Acknowledgment** This work is supported by the Singapore National Research Foundation CRP grant (Nonvolatile memory and logic integrated circuit devices, NRF-CRP9-2011-01).

- 1) S. S. P. Parkin, M. Hayashi, and L. Thomas, *Science* **320**, 190 (2008).
- 2) D. A. Allwood, G. Xiong, C. C. Faulkner, D. Atkinson, D. Petit, and R. P. Cowburn, *Science* **309**, 1688 (2005).
- 3) S. Ladak, D. E. Read, G. K. Perkins, L. F. Cohen, and W. R. Branford, *Nat. Phys.* **6**, 359 (2010).
- 4) P. Mellado, O. Petrova, Y. C. Shen, and O. Tchernyshyov, *Phys. Rev. Lett.* **105**, 187206 (2010).
- 5) E. Mengotti, L. J. Heyderman, A. F. Rodriguez, F. Nolting, R. V. Hugli, and H. B. Braun, *Nat. Phys.* **7**, 68 (2011).
- 6) Y. Shen, O. Petrova, P. Mellado, S. Daunheimer, J. Cumings, and O. Tchernyshyov, *New J. Phys.* **14**, 035022 (2012).
- 7) O. Tchernyshyov and G. W. Chern, *Phys. Rev. Lett.* **95**, 197204 (2005).
- 8) A. Pushp, T. Phung, C. Rettner, B. P. Hughes, S.-H. Yang, L. Thomas, and S. S. P. Parkin, *Nat. Phys.* **9**, 505 (2013).
- 9) K. Zeissler, S. K. Walton, S. Ladak, D. E. Read, T. Tyliszczak, L. F. Cohen, and W. R. Branford, *Sci. Rep.* **3**, 1252 (2013).
- 10) M. J. Donahue and D. G. Porter, OOMMF User's Guide, Version 1.0 Interagency Report NISTIR 6376 (National Institute of Standards and Technology, Gaithersburg, MD, 1999).
- 11) H. T. Zeng, D. Read, L. O'Brien, J. Sampaio, E. R. Lewis, D. Petit, and R. P. Cowburn, *Appl. Phys. Lett.* **96**, 262510 (2010).
- 12) C. H. Marrows, *Adv. Phys.* **54**, 585 (2005).
- 13) S. Goolaup, S. C. Low, M. Chandra Sekhar, and W. S. Lew, *J. Phys.: Conf. Ser.* **266**, 012079 (2011).
- 14) E. R. Lewis, D. Petit, A.-V. Jausovec, L. O'Brien, D. E. Read, H. T. Zeng, and R. P. Cowburn, *Phys. Rev. Lett.* **102**, 057209 (2009).
- 15) T. Shinjo, T. Okuno, R. Hassdorf, K. Shigeto, and T. Ono, *Science* **289**, 930 (2000).